ACS APPLIED NANO MATERIALS
Cite This: ACS Appl. Nano Mater. 2018, 1, 2356−2367
Article
www.acsanm.org

Controlled Growth of MoS_2 Flakes from in-Plane to Edge-Enriched 3D Network and Their Surface-Energy Studies

Abhay V. Agrawal,[†] Naveen Kumar,[†] Swaminathan Venkatesan,[‡] Alex Zakhidov,[‡] Christopher Manspeaker,[§] Zhuan Zhu,[∥] FC Robles Hernandez,[∥] Jiming Bao,[∥] and Mukesh Kumar*[,†]

[†]Department of Physics, Indian Institute of Technology Ropar, Rupnagar 140001, Punjab, India
[‡]Department of Physics and [§]MSEC, Texas State University, San Marcos, Texas 78666, United States
[∥]Department of Electrical and Computer Engineering, University of Houston, Houston, Texas 77204, United States

Supporting Information

ABSTRACT: Controlled and tunable growth of chemically active edge sites over inert in-plane MoS_2 flakes is the key requirement to realize their vast number of applications in catalytic activities. Thermodynamically, growth of inert in-plane MoS_2 is preferred due to fewer active sites on its surface over the edge sites. Here, we demonstrate controlled and tunable growth from in-plane MoS_2 flakes to dense and electrically connected edge-enriched three-dimensional (3D) network of MoS_2 flakes by varying the gas flow rate using *tube-in-tube* chemical vapor deposition technique. Field emission scanning electron microscope results demonstrated that the density of edge-enriched MoS_2 flakes increase with increase in the gas flow rate. Raman and transmission electron microscopy analyses clearly revealed that the as-synthesized in-plane and edge-enriched MoS_2 flakes are few layers in nature. Atomic force microscopy measurement revealed that the growth of the edge-enriched MoS_2 takes place from the in-plane MoS_2 flakes. On the basis of the structural, morphological, and spectroscopic analysis, a detailed growth mechanism is proposed, where *in-plane* MoS_2 was found to work as a seed layer for the initial growth of edge-enriched vertically aligned MoS_2 flakes that finally leads to the growth of interconnected 3D network of edge-enriched MoS_2 flakes. The surface energy of MoS_2 flakes with different densities was evaluated by sessile contact angle measurement with deionized water (polar liquid) and diiodomethane (dispersive liquid). Both liquids show different nature with the increment in the density of the edge-enriched MoS_2 flakes. The total surface free energy was observed to increase with increase in the density of edge-enriched MoS_2 flakes. This work demonstrates the controlled growth of edge-enriched vertically aligned MoS_2 flakes and their surface-energy studies, which may be used to enhance their catalytic activities for next-generation green fuel production.

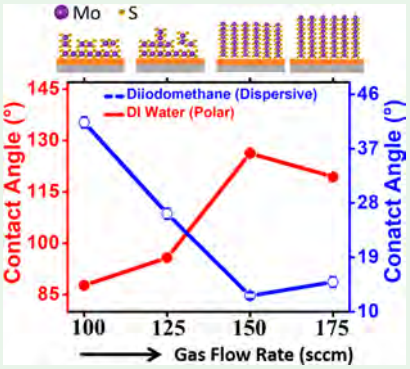

KEYWORDS: *edge-enriched MoS_2 flakes, surface free energy, growth mechanism, CVD, contact angle*

INTRODUCTION

Two-dimensional (2D) transition-metal dichalcogenides (TMDCs), especially MoS_2, have become research focus of scientific community owing to their unique electronic, physical, and chemical properties of atomically thin monolayer in contrast to their bulk counterpart and other 2D materials.[1−4] MoS_2 monolayer has a direct band gap of 1.8 eV,[4] which opens chances for its application in optoelectronics,[2] solar cells,[5] water disinfection with visible light,[6] and high ON−OFF ratio for next-generation nanoelectronic device applications.[7] Moreover, MoS_2 has demonstrated potential application in catalytic activities like highly sensitive sensors, solar hydrogen production, electrochemical catalysis, and fuel cells.[8−10]

To meet the next-generation clean-energy requirement, MoS_2 is being investigated in detail for noble-metal free electrocatalyst in hydrogen evolution reaction.[8,9,11] To enhance the catalytic activity of MoS_2, the active edge sites are preferred over the inert in-plane MoS_2.[9] Therefore, exposing more edges of MoS_2 flakes by controlling its nanostructure allows the formation of more active electrocatalyst sites. However, thermodynamics favors the presence of in-plane growth, limiting the number of active sites at the MoS_2 surface. For hydrogen evolution reaction, the control density of the defects or edge-enriched MoS_2 flakes is critical. Therefore, controlled growth with variable density of edge-enriched MoS_2 flakes and understanding their growth mechanism would be one step closer to realize their great potential in catalytic applications.

To the best of our knowledge, there are limited reports in the literature to grow edge-enriched MoS_2 flakes, while there is no detailed report to grow controlled density of vertically aligned edge-enriched MoS_2 flakes, which may limit their great potential for different catalytic applications.[12−15] Various

Received: March 23, 2018
Accepted: April 20, 2018
Published: April 20, 2018

DOI: 10.1021/acsanm.8b00467
ACS Appl. Nano Mater. 2018, 1, 2356−2367

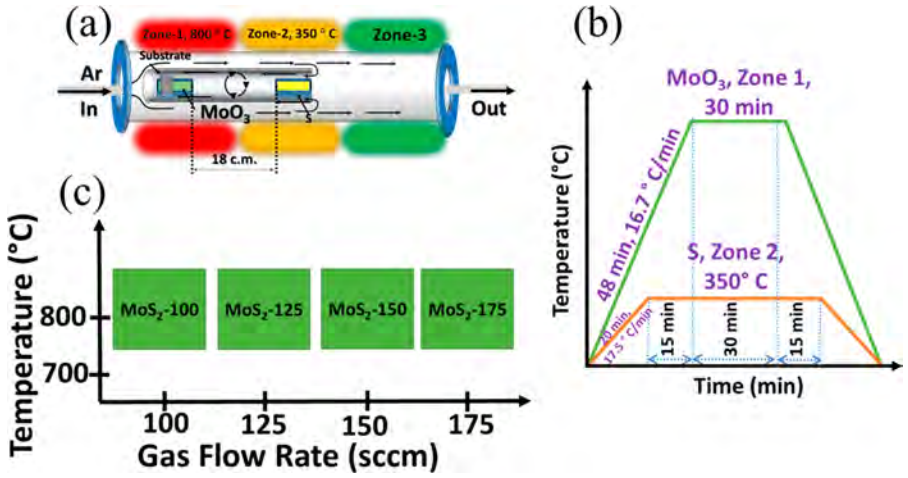

Figure 1. (a) Schematic of *tube-in-tube* APCVD technique used to grow edge-enriched vertically aligned MoS_2 flakes. SiO_2/Si substrate was placed on top of MoO_3 powder in zone 1, (b) temperature profile for MoO_3 and S powders in zone 1 and zone 2, respectively, and (c) the different growth conditions and nomenclatures of synthesized samples.

methods have been developed to synthesize different morphologies of MoS_2 materials.[16,17]

It has been reported that MoS_2 flakes can be grown via hydrothermal synthesis or using molybdenum chloride as a precursor material.[18−20] Furthermore, heterostructure growth of flowerlike structures has also been reported using graphene oxide as the template in a hydrothermal-assisted synthesis.[21,22] On the one hand, these techniques, especially hydrothermal process, involve reaction times of over 12−24 h in addition to the use of dangerous precursors such as molybdenum chloride, which could potentially form harmful chloride vapors.[22] On the other hand, atmospheric pressure chemical vapor deposition (APCVD) method has been reported for the growth of MoS_2 nanostructures including MoS_2 2D flakes via sulphurization or decomposition of predeposited metal-based precursors or one-step reaction and deposition of gaseous metal and chalcogen feedstocks.[23−30] The MoO_3 powder and S powder has been used as Mo and S source and heated at different temperatures in the simple APCVD chamber at atmospheric pressure.[20] The temperature gradient during growth and other parameters was found to impact the growth of MoS_2 nanostructures.[31] These reports clearly showed the growth of either in-plane or edge-enriched MoS_2 flakes. However, there is no controlled and successive growth from in-plane to edge-enriched MoS_2 reported in literature.

In this work, we describe the large scale, uniform, and highly reproducible controlled growth from in-plane MoS_2 to edge-enriched MoS_2 in a modified tube-in-tube APCVD technique. The MoS_2 flakes were grown at different gas flow rates to control their density from standing alone MoS_2 flakes to well-connected three-dimensional (3D) MoS_2 flakes network. The detailed morphology, structural, and optical analyses of MoS_2 flakes revealed that the growth of vertical MoS_2 flakes starts from in-plane MoS_2, and with increase in gas flow rate, the density of edge-enriched MoS_2 flakes increases to a certain limit of gas flow followed by the growth of bigger flakes at higher gas flow rate. The growth of edge-enriched MoS_2 was also achieved on varieties of the substrates like SiO_2/Si, p-doped silicon, quartz, carbon fiber, and tungsten sheet using MoO_3 and S precursors. Finally, the surface energy of variable-density edge-enriched MoS_2 flakes was calculated by using polar and dispersive liquids in sessile drop contact angle. The results reveal that the surface free energy of edge-enriched MoS_2 flakes is higher than in-plane MoS_2 layers. These results showed the method to grow control density of MoS_2 flakes and their surface-energy studies, which may be useful for next-generation hydrogen evolution reaction and their optimization.

EXPERIMENTAL SECTION

Synthesis of in-Plane MoS_2 Flakes to Edge-Enriched MoS_2 Flakes. The edge-enriched MoS_2 few layers with controlled density were synthesized on SiO_2/Si substrate using modified tube-in-tube growth chamber in the APCVD process. Before the growth, substrates were sonicated in acetone for 20 min and immediately cleaned with the nitrogen jet. High-purity MoO_3 (99.97%, Sigma-Aldrich) and sulfur powder (99.98%, Sigma-Aldrich) were loaded into two separate zirconia boats and placed in a small quartz tube closed at one end and open at other end having a diameter of 36 mm and length of 250 mm. This small quartz tube was inserted in a big quartz tube having a diameter of 55 mm and a length of 900 mm as shown in Figure 1a. The clean substrate was placed on the top of the boat containing MoO_3 powder at the closed end of the smaller tube, while the sulfur powder was placed at the opposite end of the small tube near the inlet of the small tube. This arrangement of small tube and precursor's boats was then placed into the three-zone APCVD furnace. The close end of the small tube, the substrate, and MoO_3 powder was in zone 1, and the open end and S powder was in zone 2. The distance between the MoO_3 and S powders was ∼180 mm. The small tube was inserted into the big tube in such a way that closed end faced inflow. The schematic of the modified tube-in-tube APCVD process is shown in Figure 1a.

The furnace was initially purged with the high flow of argon (Ar; 300 sccm) for 20 min to fill the growth chamber with inert gas and prevent any other atmospheric gas reaction during the growth. After the furnace was purged, Ar flow rate was reduced and set according to different growth conditions. Zone 2 was heated first to create a sulfur-rich environment in the growth chamber. When the temperature of zone 2 reached 180 °C, zone 1 containing MoO_3 powder was also heated. The heating rates for zones 1 and 2 were 16.7 and 17.5 °C/min, respectively. The ramp rates for zones 1 and 2 are shown in Figure 1b. The growth temperature condition of the zones 1 and 2 was also set according to different growth condition. During growth, the temperature of the zone 3 reached 90 °C due to heat transfer from the zone 2 to zone 3. Growth time was 30 min in all the conditions followed by cooling to room temperature in argon ambient.

Nomenclature of As-Synthesized MoS_2 Sample. The nomenclature for the grown samples is shown in Figure 1c. The MoS_2 samples were synthesized at four different gas flow-rate conditions 100 sccm (MoS_2-100), 125 sccm (MoS_2-125), 150 sccm

DOI: 10.1021/acsanm.8b00467
ACS Appl. Nano Mater. 2018, 1, 2356−2367

(MoS_2-150), and 175 sccm (MoS_2-175). The gas flow rate for samples MoS_2-100 to MoS_2-175 was changed from 100 to 175 sccm with the interval of 25 sccm to study the effect of gas flow rate on MoS_2 growth at the fixed temperatures of 800 °C for zone 1 and 350 °C for zone 2, respectively.

Characterization of Synthesized MoS_2 Sample. The grown MoS_2 samples were characterized by using field emission scanning electron microscope (FE-SEM) and Raman and photoluminescence (PL) spectroscopies. FE-SEM imaging was performed using FEI Helios NanoLab 400 with a probe current of 0.34 nA and 10 kV of an accelerating voltage. The FEI Helios NanoLab 400 is equipped with energy-dispersive X-ray spectroscopy (EDS). The PL and Raman spectra were measured using a home-built micro-PL/Raman system consisting of HORIBA iHR 320 Spectrometer equipped with Synapse CCD, 532 nm continuous-wave laser, and a 100× objective lens. The 532 nm laser was used as the excitation source, and its power was fixed at 500 μW to avoid any heating to the samples. The laser spot size was ~0.5 μm. The same sample area was used for both PL and Raman measurements. The measurements were performed under ambient condition (25 °C and 45% relative humidity (RH)). The silicon 519 cm^{-1} Raman peak was used as the reference for the system calibration. The laser wavelength setting in the spectrometer software was fine-tuned, until the laser line and silicon Raman peak line are at 0 and 519 cm^{-1}, respectively. Before the measurements, system was calibrated against the standard silicon peak at 519 cm^{-1} for all four MoS_2 samples.

X-ray photoelectron spectroscopy (XPS) measurements were conducted using a high-resolution (HR) Gammadata Scienta SES-2002 operating in an ultrahigh vacuum and using SES software 1.2.5. A monochromatic Al X-ray source (1486.6 eV, anode operating at 12 kV and 150 W) was used as the incident radiation source. Survey scans were done on each sample at a pass energy of 100 eV prior to the elemental scans. Pass energy for the elemental scans was varied from 20 to 50 eV depending on the sample.

X-ray diffraction (XRD) measurements were conducted using the Rigaku Smart Lab X-ray Diffractometer using the Smart lab Guidance software. A Cu X-ray source operating at 40 kV and 44 mA was used as the incident radiation source and operated in the Bragg–Brentano high-resolution configuration. The HR-TEM images were made in a JEOL 2000 FX TEM operated using an accelerating voltage of 200 kV with a 0.28 nm resolution. The samples were prepared from scratching the MoS_2 film deposited over the Si substrate over a holey carbon Cu grid 300 mesh.

Contact Angle Measurements. The surface wetting properties of edge-enriched MoS_2 flakes with variable density were measured with fully automatic and computer-controlled contact angle measurement setup (Apex Instruments (ACAM-S1)). The contact angle measurement system was equipped with automatic droplet dispenser for precise and accurate measurement. The droplet size was kept at 3 μL to avoid the effect of gravity on the measurement. Further, surface energies for different MoS_2 samples were calculated by using Fowkes method. The contact angle with both the liquids was performed at multiple places on 1 × 2 cm^2 substrate size, and an average value of contact angle is reported.

RESULTS AND DISCUSSION

FE-SEM results of MoS_2 flakes grown at 100, 125, 150, and 175 sccm gas flow rate at 800 °C in modified APCVD system are shown in Figure 2. It is clear from the FE-SEM image in Figure 2a that isolated edge-enriched MoS_2 flakes are observed at 100 sccm gas flow rate. A few of the flakes are combined and form starlike structures. In MoS_2-125 sample, Figure 2b, the density of edge-enriched MoS_2 flakes increases in patches, while in MoS_2-150 sample, Figure 2c, the density increases more uniformly. As the gas flow rate increases to 175 sccm, a well-connected 3D network of edge-enriched MoS_2 flakes were observed, Figure 2d. It has been observed from the SEM images in MoS_2-100 and MoS_2-175 sample, that the flake sizes are

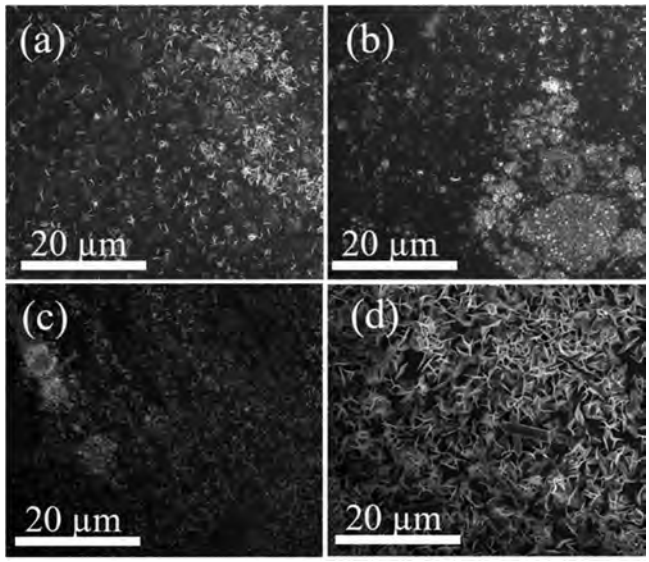

Figure 2. FE-SEM images of edge-enriched MoS_2 flakes grow at different gas flow rates of (a) 100, (b) 125, (c) 150, and (d) 175 sccm. The growth temperature for all these samples was fixed at 800 °C.

larger in nature than MoS_2 flakes for MoS_2-125 and MoS_2-150 samples. Because of larger size of the MoS_2 flakes in MoS_2-175 sample, the density of the edge-enriched MoS_2 flakes is lower in comparison to MoS_2-150. To analyze the edge-enriched MoS_2 flakes more closely, high-resolution imaging was performed, and FE-SEM images are shown in Figure 3a–d.

Figure 3a shows the FE-SEM image at MoS_2-100 sample and reveals less dense nature of edge-enriched MoS_2 flakes. For MoS_2-125 sample, flakes become more connected and dense, while with further increase in gas flow rate the density of edge-enriched MoS_2 flakes increases more uniformly. However, it was observed that the MoS_2 flakes grow bigger in size for the

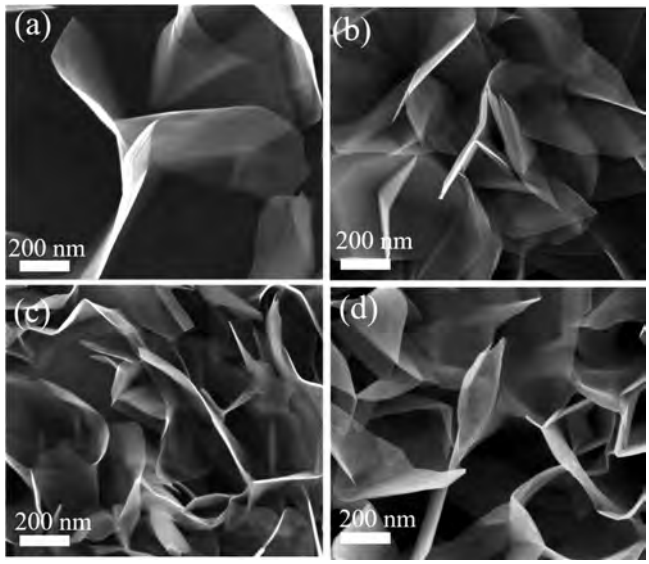

Figure 3. HR FE-SEM images of edge-enriched MoS_2 sample grown at (a) 100, (b) 125, (c) 150, and (d) 175 sccm argon flow and at 800 °C temperature. FE-SEM images clearly revealed the density of MoS_2 flakes is increased continuously from MoS_2-100 and MoS_2-125 to MoS_2-150, while the size of flakes is increased for MoS_2-175 with comparatively lower density.

DOI: 10.1021/acsanm.8b00467
ACS Appl. Nano Mater. 2018, 1, 2356–2367

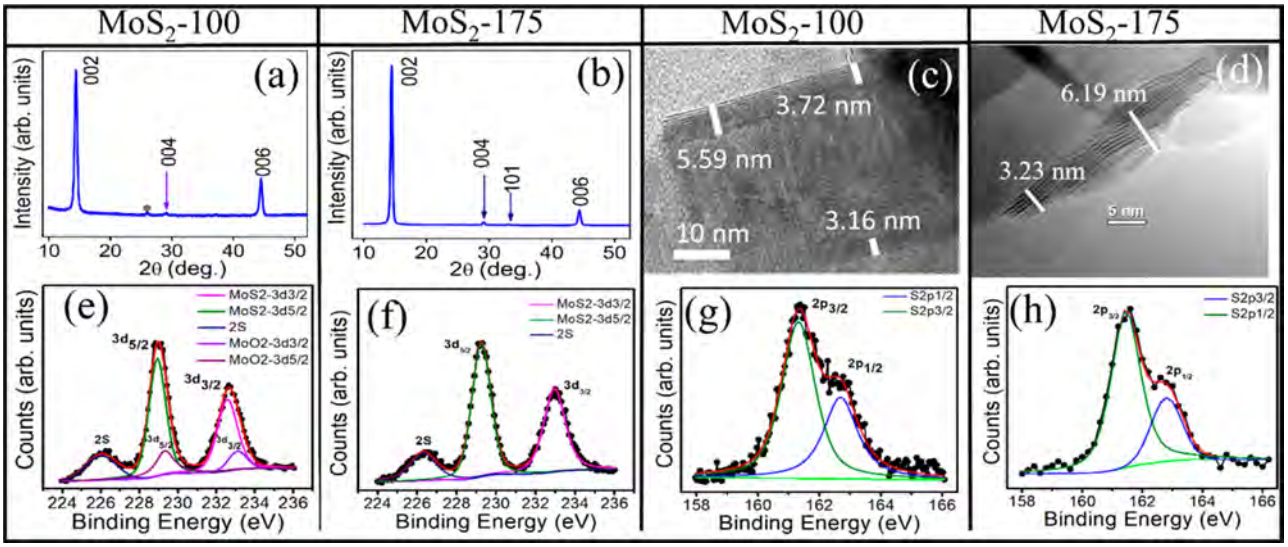

Figure 4. (a, b). XRD spectra acquired from the sample MoS_2-100 and MoS_2-175. (c, d) Cross-sectional TEM images of edge-enriched flakes obtained from the MoS_2-100 and MoS_2-175 sample. XPS scan of the samples. (e–h) HR elemental scan for Mo and S for MoS_2-100 and MoS_2-175.

MoS_2-175 sample, and the number of edge-enriched flakes per unit area decreased. The optical images and the color contrast of the as-synthesized four samples is shown in the Supporting Information (Figure S1). The SEM images shown in Figure S1 clearly revealed the quality of the uniform growth of as-prepared MoS_2 flakes on four samples over the large area. The uniform growth area of the as-synthesized MoS_2 flakes varied from 1 × 2 cm^2 to 1 in^2 on SiO_2/Si substrate.

The tube-in-tube arrangement plays an important role to achieve uniform and controlled growth of MoS_2 flakes on large area. In one tube circular CVD setup the gas fluid has the maximum velocity at the center of the tube and zero velocity at the surface of the tube wall. So, the diffusion of the precursors is very high, which led to the fast and random nucleation of the MoS_2 on the substrate.[24,29,30] However, in tube-in-tube arrangement, the gas flow rate is very smaller at the closed end of the small tube than the gas velocity at the inlet of small tube.[32] Thus, MoS_2 vapor formed by the vaporization of the S and MoO_3 powder deposited slowly on the substrate. Therefore, the tube-in-tube setup plays an important role to control the nucleation density and the uniformity even over the large region.

The growth of MoS_2 flakes under optimized condition for edge-enriched flakes (175 sccm and 800 °C) was repeated on different substrates like carbon fiber, highly doped p-type Si, W sheet, and quartz substrates. We observed uniform and large area (1 × 2 cm^2) growth of edge-enriched MoS_2 flakes. The optical images and FE-SEM images of MoS_2 flakes grown on the varieties of substrates are shown in Figure S2 of Supporting Information. The surface morphology of MoS_2 flakes clearly reveals that the present study is highly reproducible to grow highly uniform MoS_2 flakes even on different substrates.

To understand and confirm the structural, morphological, and chemical compositions of the as-grown MoS_2 samples, we performed and analyzed XRD on all four samples. TEM and XPS were performed only for the two extreme samples MoS_2-100 and MoS_2-175. The MoS_2-100 sample contains the mostly in-plane MoS_2 flakes, and as we increased the gas flow rate, the density of edge-enriched MoS_2 flakes increases, and MoS_2-175 sample contains highly uniform and dense edge-enriched MoS_2 flakes. Thus, we chose these two extreme samples. Figure 4 shows the XRD, cross-sectional TEM, and XPS results.

The XRD spectra for the sample MoS_2-100 and MoS_2-175 are shown in Figure 4a,b. In MoS_2-100, three peaks are observed, namely, two high intense peaks and one weak peak at 14.40°, 44.5°, and 29.08°. These peaks are for the plane of MoS_2 corresponding to the (002), (006), and (004) with respect to the JCPDS Card No. 37-1492. The (002) peak is representative for the out-of-plane MoS_2.[33] One very small peak, which may be due to reduced MoO_3, is also observed at 26.00°, marked with star. During the synthesis, MoO_3 powder first converts to the reduced MoO_3 followed by the sulfurization process, which results in the MoS_2 formation. The possible chemical reaction is given in eqs 1 and (2).[34−36]

$$2MoO_3 + S \rightarrow 2MoO_2 + SO_2 \quad (1)$$

$$MoO_2 + 3S \rightarrow MoS_2 + SO_2 \quad (2)$$

For MoS_2-175, we are getting the four peaks 14.40°, 29.03°, 33.07°, and 44.29°, which correspond to (002), (004), (101), and (006) planes. The peak corresponding to MoO_2 is completely disappeared, which clearly shows the increase in the uniformity of the MoS_2. Furthermore, the peaks in the case of the MoS_2-175 become more intense and sharp. The XRD corresponding to the other two samples MoS_2-125 and MoS_2-150 is shown in Figure S4 in the Supporting Information. The intensity of (002) peak is increased with increase in the density of the edge-enriched MoS_2 flakes.[14,37]

The typical cross-sectional TEM performed on MoS_2-100 and MoS_2-175 samples to determine the number of the layers in the flakes are shown in Figure 4c,d.[26] Figure 4c shows that the edge-enriched MoS_2 flakes of different thickness ranging from 1.98 to 4.08 nm implies that MoS_2-100 sample has 3−6 layers of edge-enriched MoS_2 flakes.[38] In the case of the MoS_2-175 sample, the cross-sectional TEM data of edge-enriched MoS_2 flakes are shown in Figure 4d. The results reveal that edge-enriched MoS_2 flakes MoS_2 flakes are of 4−8 layers, in nature. Therefore, as the gas flow rate increases the number of layer in edge-enriched flakes may be increasing.

The great majority of edge-enriched MoS_2 flakes MoS_2 nanosheets have thicknesses varying from 3.15 to 5.6 nm

DOI: 10.1021/acsanm.8b00467
ACS Appl. Nano Mater. 2018, 1, 2356−2367

having an average d-spacing of $d = 0.62 \pm 0.1$ nm that is characteristic of the (001) plane of MoS_2 having a $P3m1$ symmetry.[39] The above results were made in more than 50 nanosheets, and here are presented only the averages and representative images to demonstrate the sample consistency. Furthermore, some of the investigated MoS_2 nanosheets are double or triple layers with thicknesses of 0.62 and 1.83 nm, respectively. Some more TEM images are shown in the Supporting Information as the Figure S5 for these two samples.

The chemical composition and stoichiometry analysis were performed for the samples MoS_2-100 and MoS_2-175 by using XPS, and results are shown in Figure 4e–h. All of the XPS data are calibrated with the adventitious carbon 1s peak at 284.8 eV. Figure 4e shows the XPS data corresponding to the MoS_2-100. The lower binding energy peak of 3d5/2 (229.1 eV) and 3d3/2 states (232.8 eV) correspond to the MoS_2, while high binding energy peak of 3d5/2 (229.5 eV) and 3d3/2 states (233.3 eV) correspond to the MoO_2. These respective 3d5/2 and 3d3/2 peaks confirm the presence of MoS_2 and MoO_2 in the MoS_2-100 sample, while in sample MoS_2-175 in Figure 4f, there is no presence of the MoO_2 seen, as the Mo 3d peaks are very sharp in nature, which reveals the single oxidation of Mo corresponding to MoS_2.

The high-resolution XPS of S 2p spectrum deconvoluted into two doublets S 2p3/2 and 2p1/2 peaks, which correspond to S^{2-} as shown in Figure 4g,h.[28] The binding energy for the S 2p3/2 and S 2p1/2 peaks were ascribed at 161.3 and 162.6 eV for the MoS_2-100 sample while at 161.4 and 162.8 eV for the MoS_2-175. The XPS analysis revealed that the chemical composition of two extreme samples, MoS_2-100 and MoS_2-175, is well matched with MoS_2.[26,40]

The MoS_2 edge-enriched flakes were characterized by Raman and PL spectroscopies, and the data are shown in Figure 5a,b.

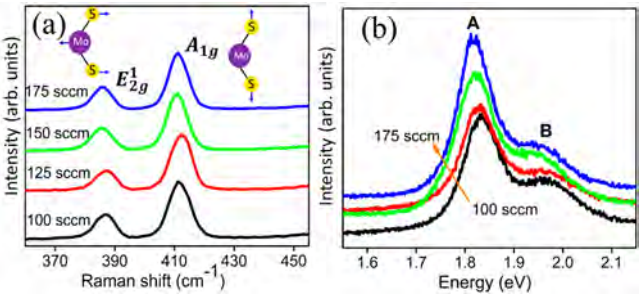

Figure 5. Representative (a) Raman and (b) PL spectra at the different positions from MoS_2 flakes samples grown at different gas flow rate. Raman spectra consist of two strong peaks that correspond to in-plane, E^1_{2g}, and out-of-plane, A_{1g}, vibrations of S–Mo–S atoms. The two PL peaks at 1.8 and 1.9 eV were observed.

Two Raman peaks near 400 cm^{-1} correspond to *in-plane* (E^1_{2g}) and *out-of-plane* (A_{1g}) vibrations of S–Mo–S atoms in MoS_2 molecules.[34] The peak position, intensity, difference of the Raman shift for the ($\Delta = A_{1g} - E^1_{2g}$) and intensity ratio ($E^1_{2g}/A_{1g}$) for two peaks in all four samples are summarized in Table 1. To check the uniformity and quality of MoS_2 flakes, Raman data were taken at different areas. The *in-plane* vibration mode was observed to vary from 384 to 388 cm^{-1}, while *out-of-plane* vibration mode was varied from 407 to 411 cm^{-1}. It is found that MoS_2 flakes grown at different gas flow rate have the frequency difference (Δ) between the two Raman modes in the range of 18–26 cm^{-1}, which indicates that the as-grown MoS_2 flakes are monolayer to few layers in nature.[41,42]

In the case of the E^1_{2g} peak, the Mo atom vibrates in in-plane and opposite to two S atoms as shown in the Figure 5a, while for A_{1g} mode Mo atom is in rest, and two S atoms vibrate in opposite direction in out-of-plane.[34] Thus, E^1_{2g} vibration preferentially excited for the terrace-terminated MoS_2 flakes, and the A_{1g} is for the edge-enriched MoS_2. So, the E^1_{2g} mode is preferred by the terrace sites, and A_{1g} mode is preferred by the edges of the MoS_2. Therefore, the intensity arises due to E^1_{2g} mode representing the existence of the in-plane MoS_2 flakes, while the intensity due to the A_{1g} mode represents the edge-enriched MoS_2 flakes.[27] As the density of the edge-enriched MoS_2 flakes increases, the intensity due to out-of-plane vibration mode A_{1g} increases. Because of increase density of the edge-enriched MoS_2, density of the in-plane MoS_2 flakes decreases, and correspondingly the intensity of the E^1_{2g} mode decreases. Hence, with increase of the edge-enriched MoS_2 flakes, the ratio of E^1_{2g} to A_{1g} decreases.[26] MoS_2 flakes synthesized at 100 sccm have the E^1_{2g}/A_{1g} ratio of ~0.58–0.47 at different areas. The high value of E^1_{2g}/A_{1g} at different areas implies the synthesized flakes in the sample are mostly *in-plane* MoS_2. At 125 sccm gas flow rate, this ratio reduces and is found to vary from 0.55 to 0.43 for different areas and confirms the growth of vertical aligned MoS_2 flakes. However, for the MoS_2 flakes synthesized at 150 and 175 sccm, E^1_{2g}/A_{1g} ratio is ~0.42–0.39 for the different areas.

This continuous decrease in the ratio shows the density of edge-enriched flakes increases with gas flow rates. The variation in frequency difference (Δ) may be due to the mixed signal from the single layer, bilayer, and few layers MoS_2 flakes. The single, dual, and a few layer MoS_2 flakes were observed under HR-TEM. The photoluminescence data of different MoS_2 flakes samples are shown in Figure 5b. In all the MoS_2 flakes grown at different conditions, we detected two peaks of different intensities. One peak (named as A) is located in the energy range of 1.82–1.84 eV, while another peak of low intensity is located in the energy range of 1.94–1.98 eV (named as B). The peak at A is due to direct excitonic transition at the

Table 1. Raman and PL Data for Different MoS_2 Samples[a]

	Raman spectroscopy						PL spectroscopy	
	position, cm^{-1}		intensity, au		$\Delta(A_{1g} - E^1_{2g})$	I (E^1_{2g}/A_{1g})	peak position, eV	
sample	E^1_{2g}	A_{1g}	E^1_{2g}	A_{1g}	cm^{-1}	au	A	B
MoS_2-100	386.6	411.2	46.9	99.3	24.6	0.47	1.83	1.98
MoS_2-125	385.3	411.1	42.9	99.9	25.7	0.43	1.82	1.95
MoS_2-150	387.6	412.3	40.3	100.1	24.7	0.40	1.82	1.94
MoS_2-175	386.1	411.1	39.7	99.7	24.9	0.39	1.82	1.94

[a]Raman data show the peak position and intensity corresponding to E^1_{2g} and A_{1g} modes along with the differences in two peaks ($\Delta A_{1g} - E^1_{2g}$) and their intensity ratio I (E^1_{2g}/A_{1g}). The peak positions for both PL signals are shown as A and B, respectively.

DOI: 10.1021/acsanm.8b00467
ACS Appl. Nano Mater. 2018, 1, 2356–2367

K-point of the Brillouin zone from K_4 to K_5, and peak B is due to exciton transition from K_1 to K_5.[43,44] The peak position for peak A and peak B and other data are listed in Table 1.

The intensity variation within the different samples may depend strongly on the various parameters like thickness, defects, strain, and heights of MoS_2 flakes.[45] To understand the growth mechanism, we closely investigated MoS_2-100 sample by using FE-SEM and Raman and PL spectroscopies, and the results are shown in Figure 6a–d. Figure 6a shows the optical

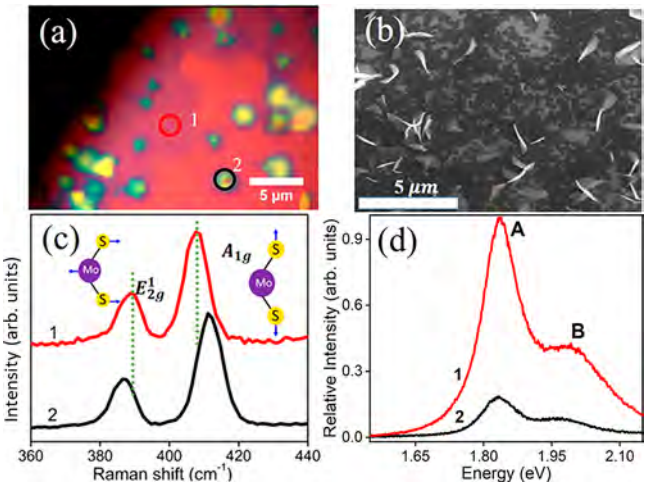

Figure 6. (a) The optical image of MoS_2-100 sample, area 1, corresponds to monolayer of MoS_2 flakes, and the area 2 corresponds to multilayer MoS_2 flakes of the same sample at different location. (b) FE-SEM image of MoS_2-100 sample. (c) Raman and (d) PL spectra recorded at the marked area of the sample.

image, and Figure 6b is FE-SEM image of MoS_2-100 sample. Figure 6c shows Raman measurements at two different areas marked as 1 and 2. At areas 1 and 2, two Raman peaks corresponding to E^1_{2g} and A_{1g} modes of vibration at the 388.5, 407.1 and 386.5, 411.1 cm^{-1}, respectively, were observed. The observed peak position is similar to previous reports.[34] The E^1_{2g} mode is red-shifted by 2.0 cm^{-1}, while the A_{1g} mode is blue-shifted by 4.1 cm^{-1} on area 2 with respect to area 1.

This shift is spotted when the number of layers in MoS_2 increases from a monolayer to few layers.[41] This behavior of a blue shift in A_{1g} mode is quite strange according to the classical model of coupled harmonic oscillator.[46] In MoS_2, van der Waals interaction is responsible for the bonding of the two consecutive layers, so the restoring force on each atom is increased with the addition of each layer. Therefore, both modes should be stiffened with increment in the number of MoS_2 layers. However, experimentally, there is a discrepancy in this prediction, and this is termed as Davydov splitting.[47,48] It reveals that frequency shift is not only affected by the van der Waals interlayer coupling but surface reconstruction and long-range Coulomb interaction also play an important role.[39,49]

The frequency difference between the E^1_{2g} and A_{1g} modes for area 1 and area 2 was found to be ~18.6 and 24.6 cm^{-1}, which were reported for monolayer and few layers of MoS_2 flakes, respectively.[41] This finding is in good agreement with the HRTEM results, where we can observe those single, double, and few layers frameworks. Figure 6d shows the photo-luminescence spectra obtained from the same areas as for Raman measurement. The relative PL intensity for the area 1 and area 2 is plotted. The two peaks A and B are at the energy 673.8 nm/1.84 eV and 627.1 nm/1.98 eV for the area 1 and 677.5 nm/1.83 eV and 632.5 nm/1.96 eV for the area 2. The Relative PL intensity for area 2 is only 18% of the PL intensity for the area 1. Thus, the higher PL intensity is further confirming the monolayer MoS_2 flakes in the area 1 and the few layer flakes in area 2. Therefore, MoS_2-100 sample is the mixture of *in-plane* monolayer and *out-of-plane* isolated few edge-enriched MoS_2 flakes.

To further explore and understand the growth mechanism of the edge-enriched MoS_2 flakes, we focus on the modified *tube-in-tube* process. It was observed that the modified *tube-in-tube* arrangement plays a vital role in the growth of edge-enriched MoS_2 flakes. The increased gas flow rates only provide an easy control for the density of flakes and with higher gas flow rates eventually formed 3D interconnected network of MoS_2 flakes seen in MoS_2-175 sample. As we can see in the Experimental Section, we used a modified *tube-in-tube* chemical vapor deposition system. The closed end of small tube is placed facing to the inflow of the gas in a big tube. The positioning of the small tube inside the larger tube results in the decrease of the gas flow rate inside the smaller tube by ~5–6 orders of magnitude than the gas flow rate/velocity at the open end of the small tube.[32] This reduces the deposition rate and allows nucleation sites to grow very slowly. Observed growth took 30 min as compared to the other reports in literature, where the growth time is much shorter, occurring in 5–10 min.

To understand the growth in detail, we proposed the following three-step process involved in the formation of 3D interconnected MoS_2 flakes from individual in-plane MoS_2 flakes: (i) precursor stage, (ii) nucleation stage, and finally (iii) growth stage. Figure 7 shows schematic and final FE-SEM image, morphology stage, of the as-grown MoS_2 sample. In the precursor stage, MoO_3 powder and S powder vaporized at the growth temperature in their respective zones and formed MoS_2 as mentioned in eqs 1 and 2. The condensed MoS_2 on the substrate was initially small in size, mostly monolayer and few

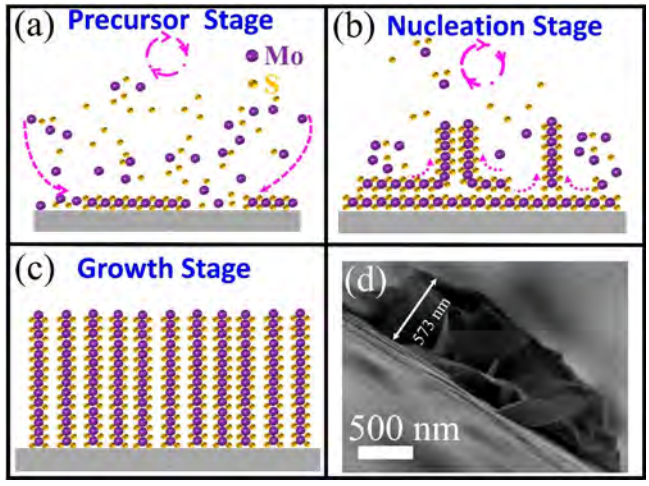

Figure 7. Proposed growth mechanism for edge-enriched MoS_2 flakes. (a) The precursor stage during the initial growth of in-plane MoS_2. In this stage of growth, in-plane MoS_2 is more, which results in monolayer to multilayer flakes formation on the substrate. (b) Nucleation stage for the growth of edge-enriched flakes. The incoming S and Mo atoms adsorbed on the substrate and on the MoS_2 flakes and start the growth of edge-enriched flakes. (c) Schematic shows the growth stage for final as-grown interconnected MoS_2 flakes. (d) Cross-sectional FE-SEM image of the edge-enriched MoS_2 flakes.

DOI: 10.1021/acsanm.8b00467
ACS Appl. Nano Mater. 2018, 1, 2356–2367

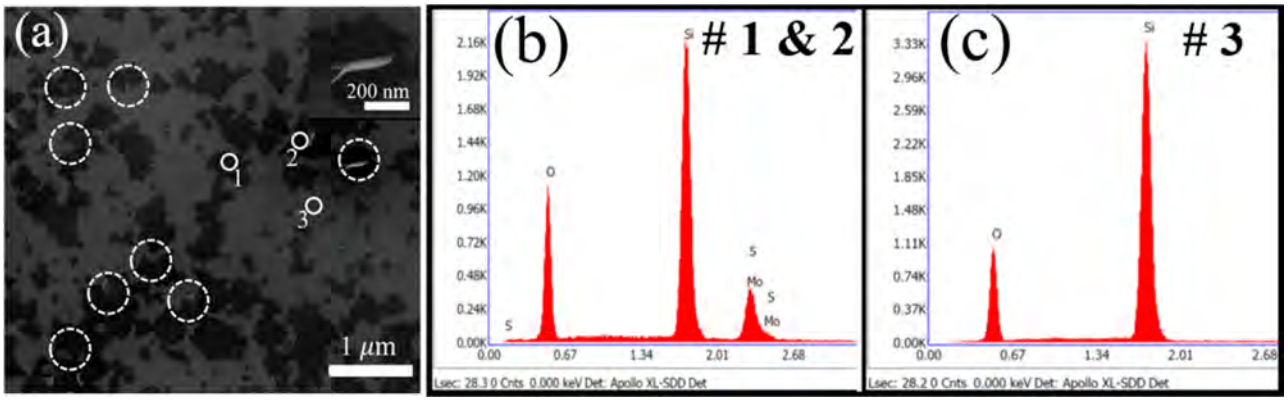

Figure 8. (a) FE-SEM image of the MoS_2-175 @ 700. (inset) The high-magnification FE-SEM image of isolated MoS_2 flakes. Spot EDS was recorded at the marked locations #1−3. (b, c) Spot EDS at locations #1 and #2 were observed similar, while EDS at base substrate site, spot #3.

layers in size, as shown in the schematic of Figure 7a. It provides the seeding platform for the further growth of edge-enriched MoS_2 flakes.

In nucleation stage, with increased growth time, the size of the condensed MoS_2 on the substrate increases, and thickness is also increased.[45] After a certain critical thickness, surface free energy increases, which also increases the strain. Thus, curling force at the boundaries effects the extension of the film and changes the alignment of the film from the 2D in-plane growth to 3D out-of-the-plane growth, as shown in the schematic of Figure 7b. The transition from 2D in-plane to vertically aligned MoS_2 flakes follows a standard Stranski−Krastanov (SK) growth model, where after forming one or more monolayer subsequent in-plane growth of MoS_2 becomes unfavorable, and island or vertically aligned MoS_2 forms. Wang et al. and others reported the synthesis of edge-enriched MoS_2 flakes using solvothermal and hydrothermal method and edge-enriched MoS_2 flakes. The MoS_2 flakes were observed to grow on the defective sites.[27,37,50,51] However, in our case, first in-plane MoS_2 flakes grow on the substrate followed by edge-enriched MoS_2 flakes due to the coalescence and changing the orientation from in-plane MoS_2 flakes to vertical MoS_2 flakes as time continues during single step. To further confirm this hypothesis, we performed atomic force microscopic measurement on in-place MoS_2 specifically where the growth of edge-enriched MoS_2 flakes just started. The AFM results, added as Figure S7 of Supporting Information, clearly reveal the layer-by-layer growth of in-plane MoS_2 and formation of edge-enriched MoS_2 on top of in-plane MoS_2 flakes.

The transition from 2D to 3D growth is not completely understood, but any factor that disturbs the monotonic decrease in the binding energy characteristic of layer growth like stress or other factors may be responsible for this.[52] Thus, the growth of edge-enriched MoS_2 flakes is the combination of the *in-plane* and *out-of-plane* growth. The *in-plane* MoS_2 flakes then provide the seeding platform for the further growth of edge-enriched MoS_2 flakes. This can be seen from Figure 7b, where edge-enriched MoS_2 flakes are grown up only where the coalescence takes place.[25,52]

To test the proposed growth mechanism and observe the onset of growth for MoS_2 edge-enriched flakes on *in-plane* MoS_2 flakes, we performed the growth of MoS_2 at a lower temperature of 700 °C and at 100 sccm keeping other conditions identical. It is observed that no deposition occurred at this condition. Keeping the temperature fixed, we increased the gas flow rate from 100 to 175 sccm. At 700 °C and 175 sccm gas flow rate, the initial growth (black patches) were found. The FE-SEM and EDS result are shown in Figure 8a−c.

Figure 8a shows the FE-SEM image of initial growth with black patches and few marked nucleation sites. It is clear from the Figure 8a that onset growth of vertically aligned MoS_2 only takes place on top of *in-plane* MoS_2 flakes. The black multilayer MoS_2 patches may be formed due to coalescing process. The coalescence process is evident from patches like structures of *in-plane* MoS_2, which may be formed due to the several mass transport mechanisms like Ostwald ripening, sintering, or cluster migration.[52]

The EDS performed at different locations is given in Figure 8b,c, which further confirms that black patches are MoS_2 flakes on the base SiO_2/Si substrate. The O peak is coming from the base SiO_2 on Si substrate. The FE-SEM results clearly indicate that *in-plane* MoS_2 grows on the substrate and acts as the seed layer for the further growth of vertically aligned MoS_2 flakes.

With higher gas flow rate, condensation of the MoS_2 increases, which leads to more coalescence of the in-plane MoS_2, resulting in more favorable seed sites for the growth of edge-enriched MoS_2 flakes. For the MoS_2-100 sample, gas flow rate is small, so the MoS_2 flakes have enough time to condense on the substrate, and they slowly formed the in-plane MoS_2 flakes. At the same time in some regions, due to coalescence, the edge-enriched MoS_2 flakes start forming as shown in Figure 2a. So, the MoS_2 vapor also started to condense at these edge-enriched MoS_2 flakes. Thus, the height of edge-enriched MoS_2 flakes increased with time.

As the gas flow rate increased to 125 and 150 sccm, in-plane MoS_2 condensed on the substrate in much less time than the samples grown up to 100 sccm and provided more seeding platform for the further growth of edge-enriched MoS_2 flakes. Thus, the coalescence takes place in different regions with the time. Therefore, instead of condensing on the edge-enriched MoS_2 flakes, MoS_2 condensed on the different regions, and the height of the edge-enriched MoS_2 flakes is small in comparison to that of MoS_2-100. Beyond 150 sccm of gas flow rate, the incoming S and Mo atoms have a higher probability to adsorb further, and this continues on the edges of MoS_2 flakes in comparison to the inert plane of vertically aligned MoS_2 flakes, which leads to larger size of MoS_2 flakes with lower density in comparison to MoS_2-150 sample. Therefore, the effective density of the edge-enriched MoS_2 in MoS_2-175 is less in comparison to MoS_2-150 sample. Figure 7d shows the side view of the edge-enriched MoS_2 flakes. The height of mostly edge-exposed flakes varies from 500 to 600 nm in all areas of the

DOI: 10.1021/acsanm.8b00467
ACS Appl. Nano Mater. 2018, 1, 2356−2367

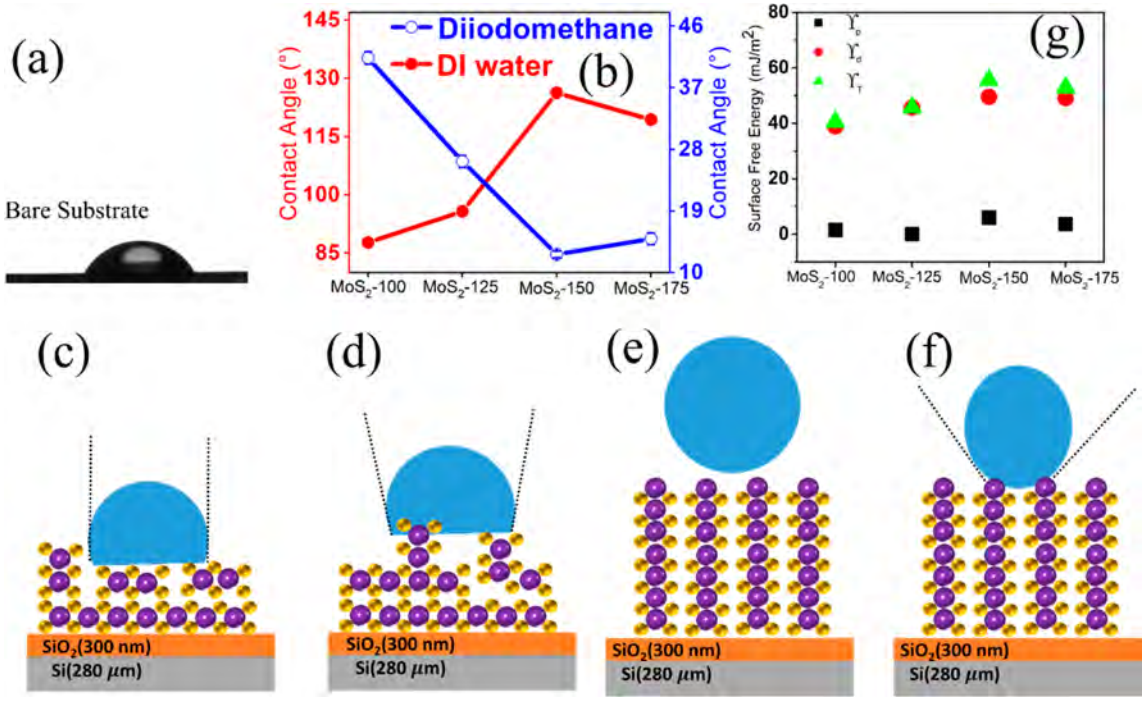

Figure 9. Wettability measurements and surface free energy study of different MoS_2 samples. Contact angle measured on (a) bare SiO_2/Si substrate with DI water. (b) Contact angle variation with DI water and diiodomethane on MoS_2 flakes synthesized at different gas flow rates. Wetting phenomenon of DI water with MoS_2 sample (c) with majority of in-plane MoS_2 (MoS_2-100) and (d) with in-plane MoS_2 and few layers of edge-enriched MoS_2 flakes (MoS_2-125). (e, f) Wensel state to Casie−Baxter state transition after the few seconds of droplet stabilization for the highly dense edge-enriched MoS_2 flakes (MoS_2-150 and MoS_2-175). (g) The variation of the total surface free energy with polar liquid and diiodomethane of MoS_2 flakes. It shows that the total surface free energy increases in controlled manner when the density of the edge-enriched MoS_2 flakes increases.

substrate. The Figure 7d and Figure 8a FE-SEM images clearly showed that the MoS_2 flakes growing on the in-plane MoS_2 are preferably vertically aligned to the substrate.

Finally, the contact angle measurements were performed on the different MoS_2 samples to understand their surface wettability and surface energies. Surface wettability is an important property of a 2D material system to understand the coating behavior, hydrogen evolution reactions, and cell proliferation.[53−57] However, surface topology, crystallinity, and chemical composition of MoS_2 films strongly affect these properties.[58−60] Previous reports observed hydrophobic nature of *in-plane* and edge-enriched MoS_2 flakes with the contact angle ranging from 87° to 98°.[31,61−63] Gaur et al. showed that the variation in contact angle was due to growth temperature and orientation of the MoS_2 film from 23° to 98°. However, prepared MoS_2 sample was atomically smooth, so the effect of the roughness is considered negligible.[60,64] Ganesh et al. observed super-hydrophobic nature of MoS_2 nanoflowers grown on graphite paper with a contact angle of 160°.[28] However, the high contact angle was attributed due to the high surface roughness of the MoS_2 nanoflower.

In this report, wettability behavior was studied by using two different liquids, namely, deionized water (DI) water (a polar liquid) and diiodomethane (a dispersive liquid). The behavior of the contact angle with a bare substrate for DI water and MoS_2 samples for two liquids is shown in Figure 9a,b.

The contact angle study for the synthesized samples with DI water shows an increase in the contact angle with the increase in the density of edge-enriched flakes, while contact angle decreased with diiodomethane for all the samples as the density of edge-enriched flakes increased. In case of the *in-plane* dominated MoS_2 sample (MoS_2-100 and MoS_2-125), the contact angle for DI water was observed around 87.6° and 95.7° Samples grown at 150 and 175 sccm show the increase in the hydrophobicity with an increase in the contact angle to 126.2° and 119.3°, respectively. The small decrease in the contact angle for the sample MoS_2-175 also revealed that the density of the flakes in MoS_2-175 sample is less in comparison to MoS_2-150 sample.

However, with diiodomethane, we obtained exactly opposite nature of wettability behavior for MoS_2 flakes. The higher value of contact angle, 41.3° and 26.2°, was observed for the sample grown at 100 and 125 sccm, while diiodomethane showed hydrophilic nature for the sample grown at 150 and 175 sccm with the contact angle of 12.6° and 14.9°, respectively. Thus, clearly DI water and diiodomethane have exactly opposite trend for the contact angle on variable-density MoS_2 flakes, and this can be attributed to the polar and dispersive nature of the liquids used. All the samples have high density of edges for a large droplet connecting region. The wetting behavior of the DI water droplets for the sample synthesized from 100 to 175 sccm is shown in Figure 9c−f. For the MoS_2 flakes at 150 and 175 sccm, density of the edge-enriched flakes is very high, and thus the contact angle increases for these samples, and droplets follow the transitions from the Casie−Baxter state to the Wensel state: decrease in contact angle with time and saturation after few seconds, as shown in Figure 9e,f. Stabilization of the droplets was studied for 10 min, and no change in the contact angle value is observed. The contact angle values for DI water and diiodomethane are affected with the variation of the density of edge-enriched MoS_2 flakes within the sample. To avoid any discrepancy that arises due to variation of

DOI: 10.1021/acsanm.8b00467
ACS Appl. Nano Mater. 2018, 1, 2356−2367

the edge-enriched MoS_2 flakes over the large area, the contact angle with both the liquids was performed at multiple locations on 1 × 2 cm^2 substrate, and an average value of contact angle is reported. The different values of the contact angle at multiple locations is tabulated in Tables S1 and S2 of the Supporting Information.

Here we proposed the controlled increase in hydrophobic nature with DI water and the increase in hydrophilic nature with diiodomethane are due to change in the orientation of MoS_2 flakes from in-plane to out-of-plane edge-enriched MoS_2 flakes. Wettability analysis measures the attraction between the liquid and solid surface, which depends mainly on adhesive and cohesive forces. The adhesive force is an attractive force observed between the solid surface and the liquid surface. Cohesive force is observed between the molecules of the liquid droplet. The dramatic behavior of MoS_2 flakes with DI water and diiodomethane can be attributed to the nature of the liquids used in the experiment. DI water is a polar solvent with the surface free energy of 72 mJ/m^2, and diiodomethane is a dispersive liquid with the surface free energy of the order 50.8 mJ/m^2 at room temperature. Polar components of surface free energy arise due to Coulombic interactions between the permanent dipoles of atoms/molecules and the induced dipoles of atoms/molecules present at the surface, while the interactions due to fluctuations of the charge distribution in the atoms/molecules give rise to the dispersive interactions.[65]

In the case of the DI water, the small increase in the contact angle value for the MoS_2-100 and MoS_2-125 is similar to previous reports for in-plane MoS_2 flakes.[31,60,62−64] The variation of the contact angle for the DI water in all four samples may be due to the surface roughness and the increased density of the edge-enriched MoS_2 flakes.[28,58,60−62] To understand more clearly, we studied the surface roughness for all four samples. To avoid any discrepancy, we measured the surface roughness at the multiple locations. The surface roughness is observed to be 87.6, 93.3, 60.4, and 55.7 nm for MoS_2-100, MoS_2-125, MoS_2-150, and MoS_2-175 samples, respectively. The data are shown in Figure S3 of the Supporting Information. It has been found that the surface roughness is higher for the samples of MoS_2-100 and MoS_2-125 in comparison to that of MoS_2-150 and MoS_2-175. However, the contact angle is higher for the samples MoS_2-150 and MoS_2-175. Thus, the surface roughness study revealed that the density of the edge-enriched MoS_2 flakes is the dominant factor to determine the contact angle value for the DI water.

The edges have the reactive sites in the form of the S vacancy, dangling bonds and the active sites.[13,28,66] DI water as a polar liquid affected these active sites, and thus the contact angle with DI water increased with these edges of the MoS_2 flakes. The small increase in the contact angle value for the samples MoS_2-100 and MoS_2-125 may be attributed to the increased density of the MoS_2 edges.[28]

In case of the diiodomethane, due to dispersive nature of the diiodomethane, contact angle with the diiodomethane is affected by the fluctuations of the charge distribution in the atoms/molecules at the surface. It has been reported that the edges of the MoS_2 behave as the metallic 1D nanowires.[31,67,68] The defects are present at the edges in the form of the S vacancies, which are produced during the growth.[69] The S vacancies are easy to produce in comparison to the Mo vacancy, since the energy required to remove the S and Mo atoms is 6.1 and 13.9 eV.[70] As the S is removed from them, the edges contain mostly the Mo atom, making them Mo-rich. As a transition metal, it has metallic nature, and it increases the conductivity of the highly uniform edge-enriched MoS_2 flakes.[67] Thus, increase in the density increases the metallic-like nature of the edges and the interaction of the diiodomethane. This may result in higher electron density at the edges of the MoS_2. MoS_2 samples grown at lower gas flow rates, 100 and 125 sccm, contain in-plane and isolated edge-enriched MoS_2 flakes as shown in Figure 2; hence, they have the less interaction.[67] The interaction of diiodomethane liquid increase more and becomes density-dependent as the density of edge-enriched MoS_2 flakes increases because of increased fluctuations in electron charge density. Because of high availability of the edges in the MoS_2-150, the contact angle is lower in comparison for all the samples.

The surface free energy of variable edge-enriched MoS_2 flakes was then measured using Fowkes methods. The surface free energy is the sum of polar and dispersive components, and surface free energy can be determined by using polar (DI water) and dispersive liquid (diiodomethane).[65] Wettability of the surface depends on the surface free energy of liquids and interaction with the solid surface.

The surface free energy of the liquid, solid−liquid, and solid is balanced by the Young's equation

$$\gamma_s = \gamma_{sl} + \gamma_l \cos\theta \tag{3}$$

where γ_s, γ_{sl}, and γ_l are the surface free energy of solid, solid−liquid, and liquids used.

In Fowkes method, surface free energy is determined by the polar and dispersive liquids. One liquid should have zero polar component like diiodomethane, $\gamma_l = \gamma_l^d = 50.8$mj/$m^2$, while the other liquid should have the sum of dominant polar and dispersive components like DI water, $\gamma_l^p = 51$ mJ/m^2, $\gamma_l^d = 21.8$ mJ/m^2, where γ_l^p and γ_l^d are the polar and dispersive component of liquid. Sum of the polar and dispersive components of interfacial energy of the solid gives the total surface energy of the solid. DI water and diiodomethane are used as the polar and dispersive liquids. Fowkes method considers the solid−liquid interactions (two-phase interactions). For system having the only dispersive components, the dispersive surface free energy component is evaluated by

$$\gamma_{sl} = \gamma_s + \gamma_l - 2(\gamma_s^d \gamma_l^d)^{0.5} \tag{4}$$

Combining eqs 3 and (4) and considering that liquid has no polar component then $\gamma_l = \gamma_l^d$ results in modified equation; the dispersive components of surface free energy can be calculated by

$$\gamma_l = \gamma_s^d = 0.25\gamma_l^d(1 + \cos\theta_d)^2 \tag{5}$$

For the liquid having both components like DI water, $\gamma_l = \gamma_p + \gamma_d$. The eq 4 has one additional polar terms

$$\gamma_{sl} = \gamma_s + \gamma_l - 2(\gamma_s^d \gamma_l^d)^{0.5} - 2(\gamma_s^p \gamma_l^p)^{0.5} \tag{6}$$

With eq 3 and eq 6, surface free energy of the polar liquid is given by

$$\gamma_s^p = \frac{[0.5\gamma_l(1 + \cos\theta_p) - ((\gamma_s^d \gamma_l^d)^{0.5})]^2}{\gamma_l^p} \tag{7}$$

where γ_l^d and γ_l^p are the dispersive and polar components of liquid, and γ_s^d and γ_s^p are the dispersive and polar components of solid.

DOI: 10.1021/acsanm.8b00467
ACS Appl. Nano Mater. 2018, 1, 2356−2367

Table 2. Measured Contact Angles and Surface Free Energy of Polar and Dispersive Liquids on the MoS_2 Surface Synthesized Using Different Conditions

	contact angle for different liquids		surface free energy by Fowkes method, mJ/m^2		
	DI water	diiodomethane			
sample	CA,[a] deg	CA,[a] deg	γ_p (polar components)	γ_d (dispersive components)	γ_T (sum of components)
MoS_2-100	87.6	41.3	1.5	38.9	40.4
MoS_2-125	95.7	26.2	0.03	45.7	45.7
MoS_2-150	126.2	12.6	6.0	49.5	55.6
MoS_2-175	119.3	14.9	3.7	49.1	52.8

[a]CA = contact angle, γ_p = polar component of surface free energy, γ_d = dispersive component of surface free energy, γ_T = surface free energy.

The calculated values of polar and dispersive components of surface free energy are shown in Table 2. Variation of polar components and dispersive components is shown in Figure 9g. Total surface free energy is also plotted, which shows the controlled variation with the density of edge-enriched MoS_2 flakes. In our case, with increasing contact angle surface free energy components for both polar and dispersive liquids decreased. However, the total surface free energy (sum of the dispersive and polar surface free energy components) increased as the density of flakes increased and has the highest value for MoS_2-150 sample. The samples MoS_2-100 and MoS_2-125, which mostly contain in-plane MoS_2 flakes, show the total surface free energy on the order of 40.4 and 45.7 mJ/m^2 and are similar to those reported in the literature for similar layer in-plane MoS_2 flakes, 46.5 mJ/m^2, while the edge-enriched flakes have the total surface free energy on the order of the 55.6 and 52.8 mJ/m^2.[31] However, no studies for the surface free energy of edge-enriched MoS_2 flakes have been done, to the best of our knowledge. In the cases of MoS_2-150 and MoS_2-175, it is observed from the SEM images shown in Figures 2 and 3 that the density of edge-enriched MoS_2 flakes is higher in MoS_2-150 in comparison to MoS_2-175. The surface free energy is the sum of the surface energy of the dispersive liquids and the polar liquids in the Fowkes method. Because of very high density of edge-enriched MoS_2 flakes in the MoS_2-150 sample, the edge-enriched MoS_2 flakes have higher effect on the surface free energy components that arises due to the diiodomethane/DI sample, as the edges have the more reactive sites in comparison to the in-plane MoS_2 flakes, and water is a polar liquid. The reactivity of the water molecules increases with the increase in the active sites; hence, the DI water contact angle increased. With the diiodomethane, increase in the edges correspondingly increase the electron concentration, which also increase the interaction of the dispersive liquid. Thus, in MoS_2-150 sample, the contact angle with DI water/diiodomethane is highest/lowest. So, the total surface free energy is also slightly higher with MoS_2-150.

CONCLUSION

In summary, controlled and tunable growth of the interconnected edge-enriched 3D network of MoS_2 flakes is reported by using modified tube-in-tube APCVD method. The MoS_2 flakes were grown at different gas flow rates to control their density from stand-alone MoS_2 flakes to well-connected 3D MoS_2 flakes network. The detailed morphology, structural, and optical analyses of MoS_2 flakes revealed that the growth of vertical MoS_2 flake starts from in-plane MoS_2, and by increases in gas flow rate the density of edge-enriched MoS_2 flakes increases. The contact angle values for DI water and diiodomethane are measured. Contact angle values for both the liquids are strongly depended upon the density of the edge-enriched MoS_2 flakes. The surface energy of MoS_2 edge structures with different density was evaluated by sessile contact angle measurement with polar (water) and dispersive (diiodomethane) liquids. The total surface free energy was observed to increase with the density of edge-enriched MoS_2 flakes. The proposed growth mechanism for edge-enriched MoS_2 flakes and their surface energy studies may be useful to design TMDC materials with desirable properties for different applications.

ASSOCIATED CONTENT

Supporting Information

The Supporting Information is available free of charge on the ACS Publications website at DOI: 10.1021/acsanm.8b00467.

Optical and FE-SEM images of the highly uniform MoS_2 samples with different gas flow rates on SiO_2/Si substrate, optical and FE-SEM images of the highly uniform MoS_2 samples on the different substrates, atomic force microscopy surface roughness measurements, XRD of MoS_2-100, MoS_2-125, MoS_2-150, and MoS_2-175 samples, cross-sectional TEM data obtained from the MoS_2-100 and MoS_2-175 samples, synthesis of MoS_2 flakes at 800° for 10 min at 150 sccm, confirmation of growth mechanism using AFM study: contact angle measurements at different locations for DI water and diiodomethane (PDF)

AUTHOR INFORMATION

Corresponding Author

*E-mail: mkumar@iitrpr.ac.in.

ORCID

Abhay V. Agrawal: 0000-0002-2940-6050
Alex Zakhidov: 0000-0001-6980-2659
Zhuan Zhu: 0000-0003-4377-9053
FC Robles Hernandez: 0000-0001-5587-0802
Jiming Bao: 0000-0002-6819-0117
Mukesh Kumar: 0000-0001-6389-2040

Notes

The authors declare no competing financial interest.

ACKNOWLEDGMENTS

We sincerely acknowledge the grant from Board of Research in Nuclear Sciences, Department of Atomic Energy, under Young Scientist Research Awards (Grant No. 34/20/09/2015/BRNS/).

REFERENCES

(1) Balendhran, S.; Walia, S.; Nili, H.; Ou, J. Z.; Zhuiykov, S.; Kaner, R. B.; Sriram, S.; Bhaskaran, M.; Kalantar-zadeh, K. Two-Dimensional

DOI: 10.1021/acsanm.8b00467
ACS Appl. Nano Mater. 2018, 1, 2356−2367

Molybdenum Trioxide and Dichalcogenides. *Adv. Funct. Mater.* **2013**, *23*, 3952−3970.
(2) Wang, Q. H.; Kalantar-Zadeh, K.; Kis, A.; Coleman, J. N.; Strano, M. S. Electronics and Optoelectronics of Two-Dimensional Transition Metal Dichalcogenides. *Nat. Nanotechnol.* **2012**, *7*, 699−712.
(3) Splendiani, A.; Sun, L.; Zhang, Y.; Li, T.; Kim, J.; Chim, C.-Y.; Galli, G.; Wang, F. Emerging Photoluminescence in Monolayer MoS2. *Nano Lett.* **2010**, *10*, 1271−1275.
(4) Mak, K. F.; Lee, C.; Hone, J.; Shan, J.; Heinz, T. F. Atomically Thin MoS2: A New Direct-Gap Semiconductor. *Phys. Rev. Lett.* **2010**, *105*, 136805.
(5) Shanmugam, M.; Durcan, C. A.; Yu, B. Layered Semiconductor Molybdenum Disulfide Nanomembrane Based Schottky-Barrier Solar Cells. *Nanoscale* **2012**, *4*, 7399−7405.
(6) Liu, C.; Kong, D.; Hsu, P.-C.; Yuan, H.; Lee, H.-W.; Liu, Y.; Wang, H.; Wang, S.; Yan, K.; Lin, D.; Maraccini, P. A.; Parker, K. M.; Boehm, A. B.; Cui, Y. Rapid Water Disinfection Using Vertically Aligned MoS2 Nanofilms and Visible Light. *Nat. Nanotechnol.* **2016**, *11*, 1098−1104.
(7) Radisavljevic, B.; Radenovic, A.; Brivio, J.; Giacometti, V.; Kis, A. Single-Layer MoS2 Transistors. *Nat. Nanotechnol.* **2011**, *6*, 147−150.
(8) Kibsgaard, J.; Chen, Z.; Reinecke, B. N.; Jaramillo, T. F. Engineering the Surface Structure of MoS2 to Preferentially Expose Active Edge Sites For Electrocatalysis. *Nat. Mater.* **2012**, *11*, 963−969.
(9) Jaramillo, T. F.; Jorgensen, K. P.; Bonde, J.; Nielsen, J. H.; Horch, S.; Chorkendorff, I. Identification of Active Edge Sites for Electrochemical H2 Evolution from MoS2 Nanocatalysts. *Science* **2007**, *317*, 100−102.
(10) Raja, R.; Sudhagar, P.; Devadoss, A.; Terashima, C.; Shrestha, L. K.; Nakata, K.; Jayavel, R.; Ariga, K.; Fujishima, A. Pt-Free Solar Driven Photoelectrochemical Hydrogen Fuel Generation Using 1T MoS2 Co-Catalyst Assembled Cds Qds/Tio2 Photoelectrode. *Chem. Commun.* **2015**, *51*, 522−525.
(11) Ye, G.; Gong, Y.; Lin, J.; Li, B.; He, Y.; Pantelides, S. T.; Zhou, W.; Vajtai, R.; Ajayan, P. M. Defects Engineered Monolayer MoS2 for Improved Hydrogen Evolution Reaction. *Nano Lett.* **2016**, *16*, 1097−103.
(12) Deokar, G.; Rajput, N.; Vancsó, P.; Ravaux, F.; Jouiad, M.; Vignaud, D.; Cecchet, F.; Colomer, J.-F. Large Area Growth of Vertically Aligned Luminescent MoS2 Nanosheets. *Nanoscale* **2017**, *9*, 277−287.
(13) Hu, J.; Huang, B.; Zhang, C.; Wang, Z.; An, Y.; Zhou, D.; Lin, H.; Leung, M. K. H.; Yang, S. Engineering Stepped Edge Surface Structures of MoS2 Sheet Stacks to Accelerate the Hydrogen Evolution Reaction. *Energy Environ. Sci.* **2017**, *10*, 593−603.
(14) Zhou, Y.; Liu, Y.; Zhao, W.; Xie, F.; Xu, R.; Li, B.; Zhou, X.; Shen, H. Growth of Vertically Aligned MoS2 Nanosheets on a Ti Substrate Through a Self-Supported Bonding Interface for High-Performance Lithium-Ion Batteries: A General Approach. *J. Mater. Chem. A* **2016**, *4*, 5932−5941.
(15) Ling, L.; Wang, C.; Zhang, K.; Li, T.; Tang, L.; Li, C.; Wang, L.; Xu, Y.; Song, Q.; Yao, Y. Controlled Growth of MoS2 Nanopetals and Their Hydrogen Evolution Performance. *RSC Adv.* **2016**, *6*, 18483−18489.
(16) Wang, S.; Rong, Y.; Fan, Y.; Pacios, M.; Bhaskaran, H.; He, K.; Warner, J. H. Shape Evolution of Monolayer MoS2 Crystals Grown By Chemical Vapor Deposition. *Chem. Mater.* **2014**, *26*, 6371−6379.
(17) Kang, K.; Xie, S.; Huang, L.; Han, Y.; Huang, P. Y.; Mak, K. F.; Kim, C. J.; Muller, D.; Park, J. High-Mobility Three-Atom-Thick Semiconducting Films with Wafer-Scale Homogeneity. *Nature* **2015**, *520*, 656−60.
(18) Tan, L. K.; Liu, B.; Teng, J. H.; Guo, S.; Low, H. Y.; Loh, K. P. Atomic Layer Deposition of a MoS2 Film. *Nanoscale* **2014**, *6*, 10584−10588.
(19) Muralikrishna, S.; Manjunath, K.; Samrat, D.; Reddy, V.; Ramakrishnappa, T.; Nagaraju, D. H. Hydrothermal Synthesis of 2D MoS2 Nanosheets for Electrocatalytic Hydrogen Evolution Reaction. *RSC Adv.* **2015**, *5*, 89389−89396.
(20) Wang, F. Z.; Zheng, M. J.; Zhang, B.; Zhu, C. Q.; Li, Q.; Ma, L.; Shen, W. Z. Ammonia Intercalated Flower-Like MoS2 Nanosheet Film as Electrocatalyst for High Efficient and Stable Hydrogen Evolution. *Sci. Rep.* **2016**, *6*, 31092.
(21) Shi, Y.; Li, H.; Wong, J. I.; Zhang, X.; Wang, Y.; Song, H.; Yang, H. Y. MoS2 Surface Structure Tailoring via Carbonaceous Promoter. *Sci. Rep.* **2015**, *5*, 10378.
(22) Yu, Y.; Li, C.; Liu, Y.; Su, L.; Zhang, Y.; Cao, L. Controlled Scalable Synthesis of Uniform, High-Quality Monolayer and few-Layer MoS2 Films. *Sci. Rep.* **2013**, *3*, 1866.
(23) Li, S.; Wang, S.; Salamone, M. M.; Robertson, A. W.; Nayak, S.; Kim, H.; Tsang, S. C. E.; Pasta, M.; Warner, J. H. Edge-Enriched 2D MoS2 Thin Films Grown by Chemical Vapor Deposition for Enhanced Catalytic Performance. *ACS Catal.* **2017**, *7*, 877−886.
(24) Gong, Y.; Lin, J.; Wang, X.; Shi, G.; Lei, S.; Lin, Z.; Zou, X.; Ye, G.; Vajtai, R.; Yakobson, B. I.; Terrones, H.; Terrones, M.; Tay, B. K.; Lou, J.; Pantelides, S. T.; Liu, Z.; Zhou, W.; Ajayan, P. M. Vertical and In-Plane Heterostructures From WS2/MoS2Monolayers. *Nat. Mater.* **2014**, *13*, 1135.
(25) Li, H.; Wu, H.; Yuan, S.; Qian, H. Synthesis And Characterization of Vertically Standing MoS2 Nanosheets. *Sci. Rep.* **2016**, *6*, 21171.
(26) Kong, D.; Wang, H.; Cha, J. J.; Pasta, M.; Koski, K. J.; Yao, J.; Cui, Y. Synthesis of MoS2 and MoSe2 Films with Vertically Aligned Layers. *Nano Lett.* **2013**, *13*, 1341−1347.
(27) Zhang, X.; Zhang, S.; Chen, B.; Wang, H.; Wu, K.; Chen, Y.; Fan, J.; Qi, S.; Cui, X.; Zhang, L.; Wang, J. Direct Synthesis of Large-Scale Hierarchical MoS2 Films Nanostructured with Orthogonally Oriented Vertically and Horizontally Aligned Layers. *Nanoscale* **2016**, *8*, 431−439.
(28) Bhimanapati, G. R.; Hankins, T.; Lei, Y.; Vila, R. A.; Fuller, I.; Terrones, M.; Robinson, J. A. Growth and Tunable Surface Wettability of Vertical MoS2 Layers for Improved Hydrogen Evolution Reactions. *ACS Appl. Mater. Interfaces* **2016**, *8*, 22190−22195.
(29) Van der Zande, A. M.; Huang, P. Y.; Chenet, D. A.; Berkelbach, T. C.; You, Y.; Lee, G.-H.; Heinz, T. F.; Reichman, D. R.; Muller, D. A.; Hone, J. C. Grains and Grain Boundaries in Highly Crystalline Monolayer Molybdenum Disulphide. *Nat. Mater.* **2013**, *12*, 554−561.
(30) Li, Y.; Dong, N.; Zhang, S.; Zhang, X.; Feng, Y.; Wang, K.; Zhang, L.; Wang, J. Giant Two-Photon Absorption in Monolayer MoS2. *Laser & Photonics Reviews* **2015**, *9*, 427−434.
(31) Gaur, A. P.; Sahoo, S.; Ahmadi, M.; Dash, S. P.; Guinel, M. J.; Katiyar, R. S. Surface Energy Engineering for Tunable Wettability Through Controlled Synthesis of MoS2. *Nano Lett.* **2014**, *14*, 4314−4321.
(32) Wang, C.; Chen, W.; Han, C.; Wang, G.; Tang, B.; Tang, C.; Wang, Y.; Zou, W.; Chen, W.; Zhang, X.-A.; Qin, S.; Chang, S.; Wang, L. Growth of Millimeter-Size Single Crystal Graphene on Cu Foils by Circumfluence Chemical Vapor Deposition. *Sci. Rep.* **2015**, *4*, 4537.
(33) Deng, J.; Yuan, W.; Ren, P.; Wang, Y.; Deng, D.; Zhang, Z.; Bao, X. High-Performance Hydrogen Evolution Electrocatalysis by Layer-Controlled MoS2 Nanosheets. *RSC Adv.* **2014**, *4*, 34733−34738.
(34) Verble, J. L.; Wieting, T. J. Lattice Mode Degeneracy in MoS_2 and Other Layer Compounds. *Phys. Rev. Lett.* **1970**, *25*, 362−365.
(35) Wieting, T. J.; Verble, J. L. Infrared and Raman Studies of Long Wavelength Optical Phonons in Hexagonal MoS2. *Phys. Rev. B* **1971**, *3*, 4286−4292.
(36) Phuc, N. H. H.; Okuno, T.; Hakiri, N.; Kawamura, G.; Matsuda, A.; Muto, H. Synthesis of High-Edge Exposure MoS2 Nano Flakes. *J. Nanopart. Res.* **2014**, *16*, 2199.
(37) Yu, H.; Yu, X.; Chen, Y.; Zhang, S.; Gao, P.; Li, C. A Strategy To Synergistically Increase the Number of Active Edge Sites and the Conductivity of MoS2 Nanosheets for Hydrogen Evolution. *Nanoscale* **2015**, *7*, 8731−8738.
(38) Ganatra, R.; Zhang, Q. Few-Layer MoS2: A Promising Layered Semiconductor. *ACS Nano* **2014**, *8*, 4074−4099.
(39) Molina-Sanchez, A.; Wirtz, L. Phonons in Single-Layer and Few-Layer MoS2 and WS2. *Phys. Rev. B: Condens. Matter Mater. Phys.* **2011**, *84*, 155413.

DOI: 10.1021/acsanm.8b00467
ACS Appl. Nano Mater. 2018, 1, 2356−2367

(40) Kumar, P.; Singh, M.; Sharma, R. K.; Reddy, G. B. Reaction Mechanism of Core−Shell MoO2 /MoS2 Nanoflakes via Plasma-Assisted Sulfurization of MoO3. *Mater. Res. Express* **2016**, *3*, 055021.
(41) Lee, C.; Yan, H.; Brus, L. E.; Heinz, T. F.; Hone, J.; Ryu, S. Anomalous Lattice Vibrations of Single and Few Layer MoS2. *ACS Nano* **2010**, *4*, 2695−2700.
(42) Li, B.; Yang, S.; Huo, N.; Li, Y.; Yang, J.; Li, R.; Fan, C.; Lu, F. Growth of Large Area Few-Layer or Monolayer MoS2 from Controllable MoO3 Nanowire Nuclei. *RSC Adv.* **2014**, *4*, 26407−26412.
(43) Eda, G.; Yamaguchi, H.; Voiry, D.; Fujita, T.; Chen, M.; Chhowalla, M. Photoluminescence from Chemically Exfoliated MoS2. *Nano Lett.* **2011**, *11*, 5111−5116.
(44) Coehoorn, R.; Haas, C.; de Groot, R. A. Electronic Structure of $MoSe_2$, MoS_2, and WSe_2. II. The Nature of The Optical Band Gaps. *Phys. Rev. B: Condens. Matter Mater. Phys.* **1987**, *35*, 6203−6206.
(45) Nan, H.; Wang, Z.; Wang, W.; Liang, Z.; Lu, Y.; Chen, Q.; He, D.; Tan, P.; Miao, F.; Wang, X.; et al. Strong Photoluminescence Enhancement of MoS2 Through Defect Engineering and Oxygen Bonding. *ACS Nano* **2014**, *8*, 5738−5745.
(46) Li, T.; Galli, G. Electronic Properties of MoS2 Nanoparticles. *J. Phys. Chem. C* **2007**, *111*, 16192−16196.
(47) Ghosh, P. N. Davydov Splitting And Multipole Interactions. *Solid State Commun.* **1976**, *19*, 639−642.
(48) Ghosh, P. N.; Maiti, C. R. Interlayer Force And Davydov Splitting in 2H - MoS_2. *Phys. Rev. B: Condens. Matter Mater. Phys.* **1983**, *28*, 2237−2239.
(49) Wieting, T. J.; Verble, J. L. Interlayer Bonding and The Lattice Vibrations of β-GaSe. *Phys. Rev. B* **1972**, *5*, 1473−1479.
(50) Zhang, S.; Yu, X.; Yu, H.; Chen, Y.; Gao, P.; Li, C.; Zhu, C. Growth of Ultrathin MoS2 Nanosheets with Expanded Spacing of (002) Plane on Carbon Nanotubes for High-Performance Sodium-Ion Battery Anodes. *ACS Appl. Mater. Interfaces* **2014**, *6*, 21880−21885.
(51) Yu, H.; Zhu, C.; Zhang, K.; Chen, Y.; Li, C.; Gao, P.; Yang, P.; Ouyang, Q. Three-Dimensional Hierarchical MoS2 Nanoflake Array/Carbon Cloth as High-Performance Flexible Lithium-Ion Battery Anodes. *J. Mater. Chem. A* **2014**, *2*, 4551−4557.
(52) Ohring, M. Film Formation and Structure. In *The Materials Science of Thin Films;* Academic Press: San Diego, CA, 1992; pp 195−247.
(53) Ma, C.-B.; Qi, X.; Chen, B.; Bao, S.; Yin, Z.; Wu, X.-J.; Luo, Z.; Wei, J.; Zhang, H.-L.; Zhang, H. MoS2 Nanoflower-Decorated Reduced Graphene Oxide Paper for High-Performance Hydrogen Evolution Reaction. *Nanoscale* **2014**, *6*, 5624−5629.
(54) Lukowski, M. A.; Daniel, A. S.; Meng, F.; Forticaux, A.; Li, L.; Jin, S. Enhanced Hydrogen Evolution Catalysis from Chemically Exfoliated Metallic MoS2 Nanosheets. *J. Am. Chem. Soc.* **2013**, *135*, 10274−10277.
(55) Chen, S.; Brown, L.; Levendorf, M.; Cai, W.; Ju, S.-Y.; Edgeworth, J.; Li, X.; Magnuson, C. W.; Velamakanni, A.; Piner, R. D.; Kang, J.; Park, J.; Ruoff, R. S. Oxidation Resistance of Graphene-Coated Cu and Cu/Ni Alloy. *ACS Nano* **2011**, *5*, 1321−1327.
(56) Wang, Y.; Li, Z.; Wang, J.; Li, J.; Lin, Y. Graphene and Graphene Oxide: Biofunctionalization And Applications In Biotechnology. *Trends Biotechnol.* **2011**, *29*, 205−212.
(57) Chen, H.; Müller, M. B.; Gilmore, K. J.; Wallace, G. G.; Li, D. Mechanically Strong, Electrically Conductive, and Biocompatible Graphene Paper. *Adv. Mater.* **2008**, *20*, 3557−3561.
(58) Drelich, J.; Miller, J. D.; Kumar, A.; Whitesides, G. M. Wetting Characteristics of Liquid Drops at Heterogeneous Surfaces. *Colloids Surf., A* **1994**, *93*, 1−13.
(59) Lopez, G.; Biebuyck, H.; Frisbie, C.; Whitesides, G. Imaging of Features on Surfaces by Condensation Figures. *Science* **1993**, *260*, 647−649.
(60) Latthe, S.; Terashima, C.; Nakata, K.; Fujishima, A. Superhydrophobic Surfaces Developed by Mimicking Hierarchical Surface Morphology of Lotus Leaf. *Molecules* **2014**, *19*, 4256−4283.
(61) Chow, P. K.; Singh, E.; Viana, B. C.; Gao, J.; Luo, J.; Li, J.; Lin, Z.; Elías, A. L.; Shi, Y.; Wang, Z.; Terrones, M.; Koratkar, N. Wetting of Mono and Few-Layered WS2 and MoS2 Films Supported on Si/SiO2 Substrates. *ACS Nano* **2015**, *9*, 3023−3031.
(62) Kelebek, S. Critical Surface Tension of Wetting and of Floatability of Molybdenite and Sulfur. *J. Colloid Interface Sci.* **1988**, *124*, 504−514.
(63) Zhang, S.; Zeng, X.; Tang, Z.; Tan, M. J. Exploring the Antisticking Properties of Solid Lubricant Thin Films In Transfer Molding. *Int. J. Mod. Phys. B* **2002**, *16*, 1080−1085.
(64) Patankar, N. A. On the Modeling of Hydrophobic Contact Angles on Rough Surfaces. *Langmuir* **2003**, *19*, 1249−1253.
(65) Fowkes, F. M. Attractive Forces At Interfaces. *Ind. Eng. Chem.* **1964**, *56*, 40−52.
(66) Jaramillo, T. F.; Jorgensen, K. P.; Bonde, J.; Nielsen, J. H.; Horch, S.; Chorkendorff, I. Identification of active edge sites for electrochemical H2 evolution from MoS2 nanocatalysts. *Science* **2007**, *317* (5834), 100−2.
(67) Bollinger, M. V.; Lauritsen, J. V.; Jacobsen, K. W.; Nørskov, J. K.; Helveg, S.; Besenbacher, F. One-Dimensional Metallic Edge States in MoS_2. *Phys. Rev. Lett.* **2001**, *87*, 196803.
(68) Agrawal, A. V.; Kumar, R.; Venkatesan, S.; Zakhidov, A.; Zhu, Z.; Bao, J.; Kumar, M.; Kumar, M. Fast Detection and Low Power Hydrogen Sensor Using Edge-Oriented Vertically Aligned 3-D Network of MoS2 Flakes at Room Temperature. *Appl. Phys. Lett.* **2017**, *111*, 093102.
(69) Lv, R.; Robinson, J. A.; Schaak, R. E.; Sun, D.; Sun, Y.; Mallouk, T. E.; Terrones, M. Transition Metal Dichalcogenides and Beyond: Synthesis, Properties, and Applications of Single- and Few-Layer Nanosheets. *Acc. Chem. Res.* **2015**, *48*, 56−64.
(70) Liu, X.; Xu, T.; Wu, X.; Zhang, Z.; Yu, J.; Qiu, H.; Hong, J.-H.; Jin, C.-H.; Li, J.-X.; Wang, X.-R.; Sun, L.-T.; Guo, W. Top−Down Fabrication of Sub-Nanometre Semiconducting Nanoribbons Derived From Molybdenum Disulfide Sheets. *Nat. Commun.* **2013**, *4*, 1776.

DOI: 10.1021/acsanm.8b00467
ACS Appl. Nano Mater. 2018, 1, 2356−2367